UNIVERSITAT POLITÈCNICA DE CATALUNYA BARCELONATECH

UPCommons

Portal del coneixement obert de la UPC

http://upcommons.upc.edu/e-prints

Aquesta és una còpia de la versió *author's final draft* d'un article publicat a la revista Chemical Engineering Journal

URL d'aquest document a UPCommons E-prints:
http://hdl.handle.net/2117/90165

Article publicat / *Published paper*:

Hermassi, M., Valderrama, C., Dosta, J., Cortina, J.L. and Batis, N.H. (2016) Detrimental effects of magnesium (II) on hydroxyapatite precipitation from synthetic industrial brines. Chemical Engineering Journal, 283. 572-581. Doi: 10.1016/j.cej.2015.07.082

1   **Detrimental effects of Magnesium (II) on hydroxyapatite precipitation from synthetic**

2   **industrial brines**

3   M. Hermassi[a,b], C. Valderrama[a], J. Dosta[c], J.L. Cortina[a] and N.H. Batis[b]

4   [a]Chemical Engineering Department. Universitat Politècnica de Catalunya-Barcelona TECH.

5   [b]Department of Biological and Chemical Engineering, National Institute of Applied Sciences and

6   Technology (INSAT), University of Carthage (Tunisia)

7   [c]Department of Chemical Engineering, Universitat de Barcelona (UB), Barcelona (Spain)

8

9   *Correspondence should be addressed to: César Valderrama

10   Departament d'Enginyeria Química, Universitat Politècnica de Catalunya

11   Av. Diagonal 647, 08028, Barcelona Spain

12   Tel.: 93 4011818, Fax.: 93 401 58 14

13   Email: cesar.alberto.valderrama@upc.edu

14

15   **Abstract**

16   The influence of Mg(II) on phosphorous recovery as hydroxyapatite (Hap) from alkaline

17   phosphate concentrates using desalinated industrial brines as the calcium source in a batch

18   reactor was evaluated. Two synthetic brines with Mg/Ca molar ratios of 2.2 and 3.3 were

19   continuously fed to reach a Ca/P molar ratio of ~1.67 to promote Hap formation under different

20   constant pH values (8, 9.5, 10.5, 11.5 and 12). For both brines, inhibition of Hap precipitation and

21   formation of the amorphous mineral phases of Ca-, Mg- and Ca/Mg-phosphates were observed at

22   pH >9.5. Mg(II) severely inhibited phosphate precipitation, allowing the formation of amorphous

23   calcium phosphate from meta-stable clusters due to Mg(II) incorporation into Ca-phosphate. For

24   the Mg/Ca (3.3) brine, a more soluble Mg-phosphate mineral (cattiite) was formed at pH 11.5.

25   Thermal treatment of the amorphous solids to increase crystallinity confirmed the presence of

Hap and chlorapatite as Ca-phosphate, stanfieldite as Ca-Mg-phosphate and farringtonite as Mg-phosphate. In the experiments at pH 8, the formation of stable nanometre-sized pre-nucleation clusters promoted nucleation inhibition, even in supersaturated solutions, and no solids were recovered after filtration. Although sulfate was involved in some of the precipitation reactions, its role in the inhibition of Hap formation is not clearly elucidated.

Keywords: phosphate recovery; brines; hydroxyapatite; stanfieldite; cattiite; farringtonite

1. Introduction

Phosphorus (P) is a non-renewable resource, non-substitutable for agriculture and food production and directly linked to global food security, as well as being important in other industrial and technical uses. At the same time, P losses are the principal contributor to eutrophication of surface waters, globally the P footprint of human diets continues to increase and the world mineral phosphate reserves decrease and there is a debate about their extent and extractability and about their geographical concentration. Improving the efficiency of P processing and use, in industry, agriculture, livestock production, food processing, and developing P reuse or recovery-recycling can reduce costs, contribute to reducing nutrient pollution, and create jobs in the frame of circular economy [1].

Phosphate is typically present at low concentrations in urban wastewaters (from 10 to 30 mg P-PO_4^{3-}/L) and in industrial wastewaters, such as detergent manufacturing, food processing or metal-coating processes (50 to 0 mg P-PO_4^{3-}/L) [2–4]. The removal of phosphate from water bodies is important because it causes eutrophication, which has a harmful effect on aquatic life, resulting in a reduction in biodiversity. On the other hand, the recovery of phosphate from phosphorus-containing wastewater is essential for developing an alternative phosphorus source to overcome the global challenge of its scarcity [5]. However, one of the disadvantages that complicates phosphate recovery is the low concentration of phosphate in the target effluents.

Many different processes have been proposed for pre-concentration of phosphate, such as adsorption, ion exchange and biological treatment [6–8]. The introduction of new P-selective sorbents (e.g., hydrated metal oxide based sorbents) would generate alkaline phosphate concentrates due to the requirements of the sorbent regeneration with NaOH solutions [6].

Chemical phosphorus recovery using Ca(II) and Mg/NH_4 salts to precipitate or crystallize phosphate as NH_4-Mg or Ca salts are the primary solutions postulated [9]. To address this objective, the use of industrial wastes as alternative Ca(II) sources for Ca-phosphate precipitation has been suggested. Ca-phosphates can be recovered by crystallization of Hap in appropriate reactors via pH and chemical dosing control, as reported previously [10-13]. Recently, the use of seawater reverse osmosis and nanofiltration brines for the recovery of economically valuable constituents [14] or specifically as an inexpensive Mg(II) and Ca(II) source, and for struvite recovery from anaerobic digesters in municipal wastewater treatment plants was suggested [15-17].

The significant Ca(II) concentration present in seawater brines (up to 0.4 g Ca/L) may enhance the precipitation of Ca-phosphate minerals (e.g., $Ca_3(PO_4)_2$ and $Ca_5(PO_4)_3(OH)$, among others). However, the influence of high concentrations of Mg(II) up to 1 g Mg(II)/L is unknown. Salami et al. [18] reported no detectable effect of Mg(II) ions on the growth of dicalcium phosphate dihydrate, but they did report that the Mg(II) ions appreciably decelerated the rate of octacalcium phosphate growth, most likely by adsorption at active growth. More recently, Cao and Harris [19] studied the interactive effects of CO_3^{2-} and Mg(II) ions on Ca-phosphate precipitation under conditions simulating dairy manure-amended soil leachate and phosphate recovery from manure wastewater. The inhibition effects of Mg(II) and the synergistic effect of both of the ions on Hap crystallinity and the precipitation rate promoted the formation of amorphous Ca-phosphate (ACP), presumably due to Mg(II) incorporation into the crystal structure. However, the presence of Mg(II) or SO_4^{2-} ions in the case of using industrial desalinated brines at concentrations higher than the

75 calcium ions has not been studied. Moreover, few studies in literature are devoted to study the

76 potential precipitation of Ca-Mg-phosphate minerals and the mechanism involved. It should be

77 mentioned the work done by Golubev et al. [20, 21] who postulated the formation of

78 $((Ca,Mg)_4H(PO_4)_3.xH_2O)$ in the precipitation of phosphate with sea water and more recently

79 Muster et al. [22] who postulated theoretically the formation of potential Ca-Mg phases.

80 Therefore, the goal of this study is to evaluate the potential inhibition of Mg(II) on hydroxyapatite

81 (Hap) precipitation during the valorisation of concentrated phosphate effluents when using

82 synthetic industrial desalinated brines as the calcium source. Two brines with different Mg/Ca

83 molar ratios of (2.2) and (3.3) were used. The precipitation/crystallization of Ca- and/or Mg-

84 phosphate processes at different constant pH values were evaluated in a batch reactor and the

85 precipitate properties were also studied. The variation of the Ca- and Mg-phosphate nucleation

86 profiles was used to elucidate the formation mechanism of Hap or Mg-phosphates with high

87 Mg(II) concentration brine.

88 **2. Materials and Methods**

89 **2.1 Experimental set-up and procedures**

90 The precipitation of phosphate (P(V)) was performed in a 2 L glass batch reactor at constant pH

91 values (8, 9.5, 10.5, 11.5 and 12), following the conditions defined in a previously study [13].

92 These alkaline pH values were selected based on the thermodynamic prediction for the

93 precipitation of Ca and Mg phosphates. Stirring at 250 rpm was achieved using a mechanical

94 stirrer (IKA RW 20). The pH was monitored on-line using a pH potentiometer (Crison pH 28),

95 when the pH was 0.1 units above or below the set point, 1 M HCl or 1 M NaOH was dosed using

96 a peristaltic pump. Batch experiments were performed by mixing a 1.0 g P-PO_4^{3-}/L solution with

97 Mg/Ca brine. NaH_2PO_4 was used to prepare the phosphate solutions. Composition was fixed

98 according to the expected conditions of the elution of ion exchange resins on the recovery of

phosphate from treated waste water effluents. Two synthetic solutions with different Mg/Ca molar ratios (2.2 and 3.3) were prepared by mixing given amounts of NaCl, $CaCl_2.2H_2O$, Na_2SO_4 and $MgCl_2.6H_2O$. The compositions of both of the brines are summarized in Table 1. The presence of antiscalants typically present on desalination brines (e.g. 1-2 mg/L) and the temperature were not included in the experimental design.

Brine solution was added at a flow rate of 0.3 mL/min (using a Gilson Minipuls 3 peristaltic pump) to reach a Ca/Pa molar ratio of 1.67 suitable for Hap precipitation. Experiments were performed at room temperature (22±2 °C) in duplicate.

Table 1.

Batch reactor aqueous samples were obtained during the experiments and then filtered through a 0.22-µm filter. The total concentrations of ions were determined by ion chromatography using an Ionex Liquid Chromatograph (ICS-1000). The accuracy of the measurements was higher than 95%. At the end of the experiments, the solid phase was removed from the reactor by filtration, washed with deionised water several times and dried at 60°C for 24 h.

2.2 Particle analysis

The solid phase particle size distribution was analysed by LS with a Coulter diffraction particle size analyser (LS 13 320 Laser Diffraction Particle Size Analyser Instrument, Beckman Coulter). The crystal size distribution range (CSD) varied from 0.04 to 2000 µm. Particles were analysed as obtained directly from the batch reactor without any thermal treatment or particle size separation.

The phase purity and crystallinity of powder were analysed by X-ray diffraction with λ CuKα radiation (λ= 1.54056 Å) at a scanning rate of 19.2 and 57.6 s, a steep angle of 0.015° and 2θ over range of 4 to 60°. The solids in powder form were identified by the Joint Committee Powder Diffraction Standards (JCPDS) file and were compared with the Powder Diffraction File (PDF) no.

123   00-009-0432 for Hap ($Ca_{10}(PO_4)_6(OH)_2$), 00-011-0231 for stanfieldite ($Ca_4Mg_5(PO4)_6$), 00-025-

124   1373 for farringtonite ($Mg_3(PO4)_2$) and 00-001-1011 for chlorapatite ($Ca_{10}Cl_2(PO4)_6$) [23].

125   To elucidate the potential inhibition mechanism, a portion of the amorphous phases was heated

126   at 1050°C for 4 h and cooled at room temperature to enhance the crystallinity of the precipitated

127   phases. It cannot been discarded that the thermal treatment promotes additionally to an increase

128   of crystallinity a change on the crystal structure or the chemical composition. However, the

129   information provided after this treatment is valued as it is improving the mechanisms discussion

130   [24].

131   **2.3 Prediction of phosphate precipitation processes**

132   Phosphate precipitation processes using Mg/Ca brines were studied using the HYDRA-MEDUSA

133   [25] and the Visual Minteq codes [26]. The measured P(V), Mg(II), Ca(II), SO_4^{2-}, and Cl^-

134   concentrations were compared when required to those estimated using both of the codes.

135   Although conditions in the precipitation tests could be far away from the equilibrium, measured

136   and predicted values were used to identify the potential reactions and mechanism involved,

137   especially when the solids formed were not appropriately characterized.

138   The supersaturation index (SI) was calculated by Visual Minteq and using Equation 1, as follows:

139      $$SI = \log \left(\frac{IAP}{K_{so}}\right)$$

140   (1)

141   where IAP is the ion activity product, and K_{so} is the solubility constant. Equilibrium solubility data

142   for Ca-Mg-phosphates were critically reviewed from the HYDRA and PHREEQ C databases, and

143   the selected values are shown in Table (S1) (Supporting Material) [11, 27, 28].

144   **3. Results and Discussion**

3.1 Influence of pH on the phosphate recovery with Ca/Mg brines

Precipitation of Hap with Mg/Ca (2.2) and Mg/Ca (3.3) brines was studied as a function of pH (8, 9.5, 10.5, 11.5 and 12). The change of total phosphate concentration and recovery (%) as a function of reaction time is shown in Figure 1 in which the dotted lines represent the expected total phosphate concentration if any precipitation reaction was involved. Phosphate recovery efficiency in the richest Mg brine (Mg/Ca 3.3) (Figure 1 c and d) is larger at pH up to 10.5. Higher recoveries were measured in only 18 hours, while for the Mg/Ca (2.2) brine were observed after 34 hours (Figure 1 a and b). A similar trend was reported by Su et al. [11] when precipitating phosphate with magnesium chloride solutions (Mg/P (2.1)) in alkaline media (pH 10, 11 and 12) in a fluidized bed reactor.

Figure 1.

The lowest phosphate recoveries (20%) were reported at pH 8 for Mg/Ca (2.2) brine and at pH 8 and 9.5 for Mg/Ca (3.3) brine. For both of the brines (at lower pH) at the end of the experiment after filtration, the solutions presented turbidity, and no precipitate was recovered on the 0.22-μm filter. This result was associated with the inhibition of the nucleation process and the formation of clusters of the nanometre size, as discussed in section 4.3.

The increase of phosphate recovery efficiency with increasing pH is explained by the change of P(V) speciation. At pH 8, 45% of P(V) is present in solution as HPO_4^{2-}, and less than 4% is present as PO_4^{3-} for the initial additions of brine with 12-8 mmol/L P(V) concentrations. However, at pH 11.5, 41% of P(V) is present as PO_4^{3-} and 20% as HPO_4^{2-}, and a higher SI is achieved. As demonstrated by Gunawan et al. [29], the degree of supersaturation and the type of precipitates formed depend on the pH. A higher pH leads to higher SI and accelerates the precipitation reaction as well as increasing its efficiency.

3.2 Influence of brine composition on Hap formation and precipitation inhibition

3.2.1 Recovery of phosphate by Mg/Ca (2.2) brines

The change of the Mg(II), Ca(II), SO_4^{2-} and Cl$^-$ contents as a function of precipitation reaction time is plotted in Figure 2 in which the solid lines represent the total ion concentration added to the reactor throughout the experiment, which is the concentration expected to be measured for a species not involved in any precipitation or solid formation reaction.

Figure 2.

As can be seen in Figure 2a, Mg(II) concentration is reduced to less than 0.2 mmol/L, independent of the pH value, while the Ca(II) concentrations are maintained below 1 mmol/L, with the exception of pH 8, where values are equal to the total added Ca(II) concentration. In the case of SO_4^{2-}, the measured concentrations agree with the total added concentration, except for the experiment at pH 8 with values below 10%. For Cl$^-$, the measured concentrations showed a reduction from 700 to 400 mmol/L. This behaviour confirms that these ions (Mg(II), Ca(II) and Cl$^-$) are involved in the precipitation reactions.

Figure 3.

The variation of the SI of the expected mineral phases along the reaction time, such as Hap, tricalcium phosphate (TCP), octacalcium phosphate (OCP), monotite and brushite for Ca(II) as well as $Mg(OH)_2$ and $Mg_3(PO4)_2$(s) for Mg(II) is shown in Figure 3 for pH 11.5 and 8. At higher pH values (9.5 and 11.5), the precipitation of Ca-phosphates is favoured (up to 90% of P(V) recovery at pH 11.5, as shown in Figure 1). The SI of the Ca-phosphate mineral phases were close to zero for brushite and monotite, close to 4 for TCP and OCP, and close to 18 for Hap (Figure 3a). Therefore, nucleation of Hap, the most stable phase among the Ca-phosphates, is expected to occur instantaneously [30]. Typically, supersaturation of Hap is achieved by a simple increase in

191   pH [31], and then it follows a three-stage process in which the initially formed amorphous ACP

192   may be redissolved and form HAP nuclei followed by formation of hydroxyapatite [32-34].

193   XRD analysis of the precipitates collected in both of the experiments at pH 9.5 and 11.5 reveals

194   that the formed Ca-phosphates were amorphous, as shown by a broad peak between 23° and

195   35° (2θ) (Figure 4a). These patterns are typical of ACP [35], indicating that Mg(II) promoted the

196   formation of the relatively unstable ACP, in the form of ACP-adsorbed Mg(II), and then hindered

197   the expected Hap formation according to the saturation indexes [36, 37].

198   **Figure 4.**

199   Yang et al. [38] reported that Mg(II) ions reduce the nucleation rate of Hap in Ca-phosphate

200   supersaturated solutions by stabilizing the gel-like ACP phase and increasing the induction and

201   transformation time. Ding et al. [37] described that Mg(II) ion adsorption onto ACP is more

202   effective than the phase incorporation at inhibiting phase transformation from ACP to Hap.

203   Additionally, at these pH values, sulfate was not involved in the formation of solid phases

204   (measured values agree with the total added concentration), and it is present in solution primarily

205   as complexed species (e.g., $MgSO_{4(aq)}$ and $CaSO_{4(aq)}$), avoiding the precipitation or re-dissolution

206   of potential Ca-phosphate precipitates [7].

207   The SEM–EDX analysis of the amorphous solids confirmed the major presence of precipitates

208   containing Ca–P–O and to a minor extent, Mg(II) and Cl⁻. Considering that the Mg(II) and Ca(II)

209   removal ratios for both of the pH values were higher than 90%, the solubility data of different

210   Ca/Mg-phosphate mineral phases ($Mg_3(PO_4)_2(s)$, $Ca_5OH(PO_4)_3(s)$) were used to predict the

211   expected P(V) concentration throughout the experiment at each given pH. For both of the pH

212   values Figures (S1 b and c) (Supporting Material), the measured P(V) concentrations were better

213   predicted when assuming the formation of Mg-phosphate minerals than when assuming the

214   formation of Ca-phosphate minerals.

215 The XRD analysis of the amorphous precipitate at pH 9.5, after treatment at 1050°C to increase

216 its crystallinity, identified the presence of a Ca-phosphate mineral (Hap ($Ca_5OH(PO_4)_3(s)$), a Ca-

217 Mg-phosphate mineral (stanfieldite ($Ca_4Mg_5(PO_4)_6$)) and a Mg-phosphate mineral (farringtonite

218 $Mg_3(PO_4)_2$) (Figure 4b). In the case of the amorphous precipitate at pH 11.5, in addition to the

219 presence of Hap and stanfieldite, a Ca-phosphate-chloride mineral (chlorapatite ($Ca_5Cl (PO_4)_3(s)$)

220 was detected (Figure 4b). Therefore, the consumption of chloride in the precipitation reactions

221 was confirmed (Figure 2), and it was also identified by EDX analysis, as described in Table (S2)

222 (Supporting Material).

223 In the experiment at pH 8 because Ca(II) was not consumed, and Mg(II) was completely

224 consumed, the P(V) recovery (up to 20%) should be associated with the formation of Mg-

225 phosphate or magnesium hydroxide. The SI indicates that the solution is not supersaturated in

226 $Mg(OH)_2(s)$ (Figure 3c); thus, the recovery of P(V) should be associated with the formation of Mg-

227 phosphate and, potentially, with the formation of minerals containing sulfate because the

228 measured values are lower than the total added concentration. A comparison of the measured

229 and expected P(V) concentration provides a good prediction of the measured P(V) concentration

230 profile considering the formation of Mg-phosphate, as shown in Figure (S1 a) (Supporting

231 Material). Although solutions were supersaturated in Hap, OCP, TCP, brushite and monotite

232 (Figure 3b), the observed Ca-phosphate mineral inhibition could be due to the formation of

233 $CaSO_4$ as a precursor because sulfate is present at a substantially higher concentration than

234 phosphate or due to the inhibition of Mg(II) ions. At the end of the experiment, no solid was

235 recovered after solution filtration because the size of the precipitate is expected to be of

236 nanometre size (ca. below 1 nm); thus, it was not possible to confirm its chemical or mineral

237 composition or the potential inhibition effect of sulfate ions.

238 **3.2.2 Recovery of phosphate by Mg/Ca (3.3) brines**

239 The change of the major ion concentration as a function of reaction time at different pH values is

240 plotted in Figure 5. Mg(II) concentration was reduced from 15 mmol/L to less than 5 mmol/L at the

241 end of the experiments at pH 9.5 and 11.5. The Ca(II) concentration was reduced to values of 1

242 mmol/L for the experiment at pH 9.5, while for the test at pH 8 and 11.5, the measured values

243 approached the total added Ca(II) concentration (4 mmol/L), indicating that Ca(II) did not

244 participate in any precipitation reaction. Sulfate concentration was reduced from 80 mmol/L to 60

245 mmol/L at the end of the experiments, indicating that sulfate was involved in the precipitation

246 reactions. The measured chloride concentrations approached the total added concentration,

247 indicating that it was not involved in any precipitation reaction, contrary to the observed behaviour

248 for Mg/Ca (2.2) brine.

249 **Figure 5.**

250 XRD analysis revealed that the solid product collected at pH 9.5 was amorphous, while at pH

251 11.5, cattiite ($Mg_3 (PO_4)_2.22H_2O$) was detected. These results confirm the profiles of Ca(II) and

252 Mg(II) shown in Figure 5 in which the Ca(II) concentration was not reduced as the experiment

253 progressed, as revealed when it was identified by EDX analysis, as summarized in Table (S2)

254 (Supporting Material).

255 **Figure 6.**

256 At pH 11.5, the solution is supersaturated in Hap; however, the higher initial magnesium

257 concentration inhibited its precipitation, and cattiite was found ($logK_{so}$=.23.1) [39] as shown in

258 Figure 6a. Note that cattiite was formed in the presence of a high Mg(II) concentration instead of

259 the less-soluble solid Hap ($logK_{so}$= 57.8) due to the effect of Mg(II) ions on the field stability of the

260 solids, promoting the precipitation of more soluble solids [40, 41]. The measured P(V)

261 concentrations were well predicted assuming the formation of cattiite, as shown in Figure (S2)

262 (Supporting Material).

The amorphous precipitate at pH 9.5 shows a broad peak between 23° and 35° (2θ) (Figure 6a) of ACP. The SEM–EDS examination of the amorphous sample detected the presence of Ca-Mg–P–O solids and the minor presence of S. The XRD analysis of the treated sample at 1050°C identified the presence of stanfieldite ($Ca_4Mg_5(PO_4)_6$)) (Figure 6 b and c), thus confirming the consumption of Mg(II) and Ca(II), as described in Figure 5. The higher Mg(II) concentration inhibits the Hap precipitation, favouring the formation of mixed Ca-Mg-phosphates, such as stanfieldite ($Ca_4Mg_5 (PO_4)_6$), as detected by XRD. Mg(II) stabilizes ACP, which is the precursor phase during Hap formation from highly supersaturated solutions [42]. It was also described that Mg(II) could be included in the precipitated solid and could modify the solids by its smaller size and greater tendency to bond covalently [43]. Lahav et al. [17] postulated that the complexation of Ca(II) ions in the precipitation of P(V) using seawater desalination brines reduces their free concentrations, thus reducing their precipitation potential and reducing the purity of the Ca-phosphates. The analysis of solids by SEM-EDX detected the presence of S and Cl, indicating their presence in the precipitates obtained at basic pH; however, XRD analysis did not detect any crystalline form.

For the experiment at pH 8, Ca(II) and Mg(II) were partially removed (approximately 10%) with a phosphate recovery of up to 20%. The SI analysis indicated that the solution is not supersaturated in $Mg(OH)_2$(s), and the removal of P(V) should be associated with the formation of Ca-Mg-phosphates and, potentially, with minerals containing sulfate, because the measured values were lower than the total added concentration. A good prediction of the measured concentrations was obtained when considering the formation of Mg- and Ca-phosphates, as shown in Figure (S2 a) (Supporting Material). Although solutions were also supersaturated in OCP, TCP, brushite and monotite, the observed inhibition could be either due to Mg(II) ions or the formation of $CaSO_{4aq}$ of $MgSO_{4aq}$ species because sulfate is present at a substantially higher concentration than phosphate. As previously described for the Mg/Ca (2.2) brine, after solution

288 filtration, no solids were recovered due to the nanometre size of the formed clusters, and it was

289 not possible to confirm its chemical or mineral composition or the potential inhibition effect of

290 sulfate ions.

291 **3.3 Evaluation of precipitation inhibition: Effects on nucleation growth kinetics**

292 According to the XRD results, it was observed that nucleation of Hap begins with the formation of

293 the ACP precursor during the early induction steps, and after a relatively long induction period, it

294 proceeds to the appearance of nuclei [44, 45]. However, in the presence of Mg(II), the formation

295 of Mg-phosphate ion-pairs reduces the P(V) species activity, thereby reducing the relative

296 supersaturation and prolonging the induction period [42]. Figure 1 shows that the change of the

297 P(V) concentration and recovery rate for pH values between 9.5 and 12 for Mg/Ca (2.2) brine and

298 between 10.5 and 12 for Mg/Ca (3.3) brine is different than for the experiments at pH 8 for Mg/Ca

299 (2.2) brine and at pH 8 and 9.5 for Mg/Ca (3.3) brine.

300 The presence of meta-stable pre-nucleation clusters (PNCs) decreases the energetic barrier,

301 thereby facilitating nucleation (pH 9.5 and 11.5), while at pH = 8, stable clusters are considered to

302 increase the barrier, thus inhibiting nucleation [46, 47].

303   **Figure 7.**

304 Phosphate precipitation can be evaluated considering the variation of the SI at pH 8, 9.5 and 11.5

305 (Figure 7) and by using the LaMer model (Appendix) describing the crystallization processes as

306 three well-defined stages. At pH 11.5, there was an initial stage in which no precipitation

307 occurred; in the second stage in which the SI reached values from 17 to 18.5, homogenous

308 nucleation occurred; and the third stage is completed with the aggregation of small particles of

309 the homogeneously nucleated material and their heterogeneous deposition [48]. For the

310 experiment at pH 9.5 from the initial additions, a supersaturation condition was observed

311 (SI>18.5), and then the homogenous nucleation and final aggregation stages followed the trend

312 defined at pH 11.5. The observed behaviour for the experiment at pH 8 (no solid was recovered)

313 is associated with the formation of stable clusters, increasing the energetic barrier, hindering

314 nucleation and achieving heterogeneous nucleation. The longer induction time for nucleation as

315 the Mg(II) ions extend the induction and transformation time [37, 38] promotes the formation of

316 nanometre-sized nuclei (Posner's clusters of 0.7 to 1.0 nm [49]). These nanometre-sized crystals

317 could not be recovered by the 0.22-μm filter.

318 To evaluate the influence of the pH and the supersaturation on the Hap nucleation kinetics, the

319 plot of $\ln(ts)$ versus $1/[\ln(1+\sigma)]^2$ was constructed for experiments with Mg/Ca (2.2) brine at pH 8

320 and 9.5, as shown in Figure 8.

321 **Figure 8.**

322 According to Equation A3 (in the appendix) the charge in the crystalline phase structures can be

323 analysed for a given system (k_n and B are constant) in terms of the variation of the slope ($k_nf(m)$).

324 As shown in Figure 8, the depicted functions can in a first approach, be fitted by two intersecting

325 straight lines with two slopes, which divide the supersaturation space into two regimes.

326 For both of the pH values (8 and 9.5), the function has a positive slope (regime 2) reaching a

327 transition point (indicated by a vertical dotted line) followed by a plateau (regime 1) with a

328 decrease of the slope. When comparing both of the experiments, a case of nucleation inhibition

329 was identified at pH 8, as was postulated by Jian et al. [50] who determined the inhibition effect

330 by the increase in the slope and the decrease of the intercept. On the other hand, for the

331 experiment at pH 9.5, a case of nucleation promotion was identified, with a factor of

332 ($k_nf(m2)=243$), referring to regime 2, which was much lower than that reported at pH =8

333 ($k_nf(m2)=760$). This result indicates that at pH 8, it is possible to reduce the nucleation barrier by

334 improving the interfacial structure correlation [47, 50]. Similar results (data not shown) were

335 obtained for the Mg/Ca (3.3) brines.

14

336   The particle size distribution in terms of volume and the number of particles for both of the Mg/Ca

337   brines at pH 11.5 is shown in Figure (S3) (Supporting Material). The number of particles with a

338   mean size (d_{50}) increases with the Mg(II) concentration from 310 nm to 1400 nm for the Mg/Ca

339   (2.2) and Mg/Ca (3.3) brines, respectively. The precipitate particle size analysis in terms of

340   volume revealed the formation of aggregates with an average equivalent diameter of

341   approximately 113 µm and 62 µm for the Mg/Ca (2.2) and Mg/Ca (3.3) brines, respectively. The

342   initially formed particles are smaller, thus having a higher tendency to aggregate due to their

343   amorphous state and small size [51]. Excess Mg(II) negatively affects the final powder crystal

344   sizes because it causes a higher supersaturation, consequently increasing the nuclei population

345   density, which suggests a higher nucleation rate. Therefore, crystals reach larger sizes, as

346   described by [52] for Hap crystallization in the presence of excess of Mg(II) ions. The obtained

347   precipitates consist of a population of nanometre-sized primary particles and a population of

348   micrometre-sized aggregates. The aggregates most likely result from the aggregation of primary

349   nanoparticles because small particles have a high surface area-to-volume ratio, resulting in a

350   high surface tension, which tends to diminish by adhering to other particles. [53].

351

4. Conclusions

353   In this study, the influence of Mg(II) ions on phosphate recovery by Hap precipitation from basic

354   solutions with desalinated industrial brines containing mixtures of Ca and Mg was confirmed.

355   For both of the Mg/Ca (2.2 and 3.3) brines at higher pH values (9.5 and 11.5), the precipitation

356   inhibition of Hap was observed, and although solutions were supersaturated, the process

357   proceeded with the formation of typically amorphous mineral phases (e.g. Ca, Mg, and Ca-Mg-

358   phosphates). The presence of meta-stable clusters decreases the energetic barrier, thereby

359   facilitating nucleation (pH 9.5 and 11.5). In the case of experiments at pH = 8, formation of stable

360 clusters increased the barrier, thus promoting nucleation inhibition, and in this case, nanocrystals

361 were formed, and solids were not recovered after filtration with a 0.22 μm filter.

362 The presence of pre-nucleation clusters in under-and super-saturated solutions and their

363 participation in the phase separation process were proposed. Mg(II) severely inhibited precipitate

364 crystallinity and the precipitation rate, allowing formation of ACP. This result is presumably due to

365 Mg(II) incorporation into the Ca(II)-phosphate structure to form a Mg(II)-substituted structure that

366 crystallized to stanfieldite $Ca_4Mg_5(PO4)_6$ upon thermal treatment to increase crystallinity.

367 According to literature, this mineral has not been postulated previously in the precipitation of

368 phosphate solutions with Mg/Ca brines. The surface adsorption of Mg(II) (rather than the

369 incorporated Mg(II)) played a critical role in regulating the transformation rate of ACP to Hap.

370 Mg(II) altered the stability of the mineral phases, and the more soluble solids were precipitated

371 (e.g., $Mg_3 (PO_4)_2.22H_2O$) at pH 11.5. Sulfate ions have a high capacity to form complexes with

372 Ca(II) and Mg(II), and participated in the precipitation reactions. However, although sulfur was

373 detected by EDX, no mineral containing sulfate was identified by XRD.

374 The use of industrial desalinated brines containing mixtures of Cd and Mg could be a suitable

375 source for the recovery of phosphate in the form of mixed Ca-Mg phosphates suitable for the

376 chemical industries producing fertilizers.

377 **Acknowledgments**

381 **5. References**

382 [1]   Communication from the commission to the European parliament, the council, the
383   european economic and social committee and the committee of the regions, Towards a
384   circular economy: a zero waste programme for Europe, Circular Economy Strategy, COM.
385   398 (2014) 1–8.

386   [2]   N.Y. Mezenner, a. Bensmaili, Kinetics and thermodynamic study of phosphate adsorption
387   on iron hydroxide-eggshell waste, Chem. Eng. J. 147 (2009) 87–96.

388   [3]   C. Barca, C. Gérente, D. Meyer, F. Chazarenc, Y. Andrès, Phosphate removal from
389   synthetic and real wastewater using steel slags produced in Europe., Water Res. 46
390   (2012) 2376–84.

391   [4]   B. Li, M.T. Brett, The impact of alum based advanced nutrient removal processes on
392   phosphorus bioavailability., Water Res. 46 (2012) 837–44.

393   [5]   T. Nur, M.A.H. Johir, P. Loganathan, T. Nguyen, S. Vigneswaran, J. Kandasamy,
394   Phosphate removal from water using an iron oxide impregnated strong base anion
395   exchange resin, J. Ind. Eng. Chem. 20 (2014) 1301–1307.

396   [6]   S. Sengupta, A. Pandit, Selective removal of phosphorus from wastewater combined with
397   its recovery as a solid-phase fertilizer., Water Res. 45 (2011) 3318–30.

398   [7]   Y. Liu, X. Sheng, Y. Dong, Y. Ma, Removal of high-concentration phosphate by calcite:
399   Effect of sulfate and pH, Desalination. 289 (2012) 66–71.

400   [8]   H. Kodera, M. Hatamoto, K. Abe, T. Kindaichi, N. Ozaki, A. Ohashi, Phosphate recovery
401   as concentrated solution from treated wastewater by a PAO-enriched biofilm reactor.,
402   Water Res. 47 (2013) 2025–32.

403   [9]   A.T.K. Tran, Y. Zhang, D. De Corte, J.-B. Hannes, W. Ye, P. Mondal, et al., P-recovery as
404   calcium phosphate from wastewater using an integrated selectrodialysis/crystallization
405   process, J. Clean. Prod. 77 (2014) 140–151.

406   [10]   Elisabeth.V.M, Keith. B, Controlled struvite crystalisation for removing phosphorus from
407   anaerobic digester sidestreams, Water Res. 35 (2001) 151–159.

408   [11]   C.-C. Su, L.D. Dulfo, M.L.P. Dalida, M.-C. Lu, Magnesium phosphate crystallization in a
409   fluidized-bed reactor: Effects of pH, Mg:P molar ratio and seed, Sep. Purif. Technol. 125
410   (2014) 90–96.

411   [12]   F. Castro, F. Rocha, J. Anto, Continuous-Flow Precipitation of Hydroxyapatite at 37 ° C in
412   a Meso Oscillatory Flow Reactor, Ind. Eng. Chem. Res. 52 (2013) 9816–9821.

413   [13]   Hermassi. M, Valderrama. C, Dosta. J, Cortina. J.L, Batis. N.H, Evaluation of
414   Hydroxyapatite crystallization in a batch reactor for the valorization of alkaline phosphate
415   concentrates from wastewater treatment plants using calcium chloride, Chem. Eng. J. 267
416   (2015) 142-152.

417   [14]   D.H. Kim, A review of desalting process techniques and economic analysis of the
418   recovery of salts from retentates, Desalination. 270 (2011) 1–8.

419   [15]   M. Telzhensky, L. Birnhack, O. Lehmann, E. Windler, O. Lahav, Selective separation of
420   seawater Mg^{2+} ions for use in downstream water treatment processes, Chem. Eng. J. 175
421   (2011) 136–143.

422 [16] Z. Bradford-Hartke, P. Lant, G. Leslie, Phosphorus recovery from centralised municipal
423   water recycling plants, Chem. Eng. Res. Des. 90 (2012) 78–85.

424 [17] O. Lahav, M. Telzhensky, A. Zewuhn, Y. Gendel, J. Gerth, W. Calmano, et al., Struvite
425   recovery from municipal-wastewater sludge centrifuge supernatant using seawater NF
426   concentrate as a cheap Mg(II) source, Sep. Purif. Technol. 108 (2013) 103–110.

427 [18] M.H. Salimi, J.C. Heughebaert, G.H. Nancollas, Crystal growth of calcium phosphates in
428   the presence of magnesium ions, Langmuir. 1 (1985) 119–122.

429 [19] X. Cao, W. Harris, Carbonate and magnesium interactive effect on calcium phosphate
430   precipitation., Environ. Sci. Technol. 42 (2008) 436–442.

431 [20] S. V Golubev, O.S. Pokrovsky, V.S. Savenko, Unseeded precipitation of calcium and
432   magnesium phosphates from modified seawater solutions, 205 (1999) 354–360.

433 [21] S. V. Golubev, O.S. Pokrovsky, V.S. Savenko, Homogeneous precipitation of magnesium
434   phosphates from seawater solutions, J. Cryst. Growth. 223 (2001) 550–556.

435 [22] T.H. Muster, G.B. Douglas, N. Sherman, a Seeber, N. Wright, Y. Güzükara, Towards
436   effective phosphorus recycling from wastewater: quantity and quality., Chemosphere. 91
437   (2013) 676–84.

438 [23] International center of diffraction data, PCPDF Win (JCPDS-ICDD) data base software,
439   (2003).

440 [24] W.L. Suchanek, K. Byrappa, P. Shuk, R.E. Riman, V.F. Janas, K.S. TenHuisen,
441   Mechanochemical-hydrothermal synthesis of calcium phosphate powders with coupled
442   magnesium and carbonate substitution, J. Solid State Chem. 177 (2004) 793–799.

443 [25] I.S.S. Puidomènech, Chemical Equilibrium Software Hydra and Medusa, Stock. Sweden.
444   (2001) Inorganic Chemistry Department.Stock. Sweden.

445 [26] J.E. Gray-Munro, M. Strong, A study on the interfacial chemistry of magnesium hydroxide
446   surfaces in aqueous phosphate solutions: influence of Ca^{2+}, Cl^- and protein., J. Colloid
447   Interface Sci. 393 (2013) 421–428.

448 [27] Nordstrom, D.K., Pulmmer,L.N.,Langmuir, D.,Busenberg.E., May,H.M.Jones,B.F.,David,L.
449   P., Revised chemical equilibrium data for major water-mineral reactions and their
450   limitations, Chem. Model. Aqueous Sysstems II. (1990) 399–413.

451 [28] D.R. Lide, Handbook of Chemistry and Physics, taylor and francis groupe, 2008.

452 [29] L.J. Gunawan.E.K, Warmadewanthi, Removal of phosphate and fluoride from
453   optoelectronic wastewater by calcite, Int.J.Technol.Manage. 12 (2010) 308–321.

454 [30] Edzwald.J, Water quality and treatment: A Handbook on drinking water, 2010.

455 [31] E.V. JONES, Mineralogical controls on phosphorus recovery from wastewaters, Nat.
456   Museum, Hist. Road, Cromwell. 65 (2001) 611–620.

457 [32] Boskey A.L. and Posner A.S., Conversion of amorphous calcium phosphate to
458 microcrystalline hydroxyapatite. A pH dependent, solution-mediated, solid-solid
459 conversion., J. Phys. Chem. 77 (1973) 2313–2317.

460 [33] J. Meyer, Phase-transformations in the spontaneous precipitation of calcium phosphate.,
461 Croat. Chem. Acta. 56 (1983) 753–767.

462 [34] Y. Sugiura, K. Onuma, Y. Kimura, H. Miura, K. Tsukamoto, Morphological evolution of
463 precipitates during transformation of amorphous calcium phosphate into octacalcium
464 phosphate in relation to role of intermediate phase, J. Cryst. Growth. 332 (2011) 58–67.

465 [35] R. Alvarez, L. A. Evans, P.J. Milham, M. A. Wilson, Effects of humic material on the
466 precipitation of calcium phosphate, Geoderma. 118 (2004) 245–260.

467 [36] X. Cao, W.G. Harris, M.S. Josan, V.D. Nair, Inhibition of calcium phosphate precipitation
468 under environmentally-relevant conditions., Sci. Total Environ. 383 (2007) 205–215.

469 [37] H. Ding, H. Pan, X. Xu, R. Tang, Toward a Detailed Understanding of Magnesium Ions on
470 Hydroxyapatite Crystallization Inhibition, Cryst. Growth Des. 14 (2014) 763–769.

471 [38] X. Yang, B. Xie, L. Wang, Y. Qin, Z.J. Henneman, G.H. Nancollas, Influence of
472 magnesium ions and amino acids on the nucleation and growth of hydroxyapatite,
473 CrystEngComm. 13 (2011)

474 [39] A. W. Taylor, A. W. Frazier, E.L. Gurney, Solubility products of magnesium ammonium
475 and magnesium potassium phosphates, Trans. Faraday Soc. 59 (1963) 1580.

476 [40] D. Jenkins, J.F. Ferguson, Chemical processes for phosphate removal, Water Res. 5
477 (1971) 369–389.

478 [41] R.D. Cusick, M.L. Ullery, B. a Dempsey, B.E. Logan, Electrochemical struvite precipitation
479 from digestate with a fluidized bed cathode microbial electrolysis cell., Water Res. 54
480 (2014) 297–306.

481 [42] X. Yang, B. Xie, L. Wang, Y. Qin, Z.J. Henneman, G.H. Nancollas, Influence of
482 magnesium ions and amino acids on the nucleation and growth of hydroxyapatite,
483 CrystEngComm. 13 (2011) 1153–1158.

484 [43] F. John, L. Mccarty, Effects of Carbonate and Magnesium on Calcium Phosphate
485 Precipitation, (1969).

486 [44] L. Wang, G.H. Nancollas, Calcium orthophosphates: crystallization and dissolution.,
487 Chem. Rev. 108 (2008) 4628–4669.

488 [45] B. Xie, T.J. Halter, B.M. Borah, G.H. Nancollas, Tracking Amorphous Precursor Formation
489 and Transformation during Induction Stages of Nucleation, Cryst. Growth Des. 14 (2014)
490 1659–1665.

491 [46] D. Gebauer, H. Cölfen, Prenucleation clusters and non-classical nucleation, Nano Today.
492 6 (2011) 564–584.

493 [47] D. Gebauer, M. Kellermeier, J.D. Gale, L. Bergström, H. Cölfen, Pre-nucleation clusters
494 as solute precursors in crystallisation., Chem. Soc. Rev. 43 (2014) 2348–2371.

495 [48] F. Lagno, G.P. Demopoulos, Synthesis of Hydrated Aluminum Phosphate , $AlPO_4,1.5H_2O$
496 ($AlPO_4\cdot H_3$), by Controlled Reactive Crystallization in Sulfate Media, (2005) 8033–8038.

497 [49] K. Onuma, A. Ito, Cluster Growth Model for Hydroxyapatite, Chem. Mater. 10 (1998)
498 3346–3351.

499 [50] H. Jiang, X.-Y. Liu, G. Zhang, Y. Li, Kinetics and template nucleation of self-assembled
500 hydroxyapatite nanocrystallites by chondroitin sulfate., J. Biol. Chem. 280 (2005) 42061–
501 42066.

502 [51] F. Castro, S. Kuhn, K. Jensen, A. Ferreira, F. Rocha, A. Vicente, et al., Process
503 intensification and optimization for hydroxyapatite nanoparticles production, Chem. Eng.
504 Sci. 100 (2013) 352–359.

505 [52] N. Hutnik, A. Kozik, A. Mazienczuk, K. Piotrowski, B. Wierzbowska, A. Matynia,
506 Phosphates (V) recovery from phosphorus mineral fertilizers industry wastewater by
507 continuous struvite reaction crystallization process., Water Res. 47 (2013) 3635–43.

508 [53] M.D. Luque de Castro, F. Priego-Capote, Ultrasound-assisted crystallization
509 (sonocrystallization)., Ultrason. Sonochem. 14 (2007) 717–724.

510

511

512

513

514

515

516

517

518

519

Appendix A. Fundamental precipitation inhibition effects on nucleation growth kinetics

Lamer and Dinegar [1] described the formation of colloidal nanocrystals in a solution phase through a crystal nucleation process involving the following three steps: i) ions start to aggregate into nuclei via self-nucleation as the monomer concentration increases in the solution to supersaturation levels, ii) monomers continuously aggregate on the pre-existing nuclei or seed, which leads to a gradual decrease in the monomer concentration, and iii) nuclei grow into nanocrystals of increasingly larger sizes until reaching an equilibrium state.

The nucleation and growth steps are two relatively separated processes, and the formation of nuclei occurs only at a reactant concentration substantially higher than the saturation concentration (C_s); otherwise, growth of the existing nuclei dominates. The subsequent growth steps will strongly govern the final morphology of the nanocrystals [2], [3] and [4].

The free energy change required for the formation of nuclei (ΔG) is determined by the free energy change for the phase transformation (ΔG_v) and the free energy change for the formation of a solid surface (ΔG_s) [5]. Then, the driving force ($\Delta\mu$) required for Hap ($Ca_5(PO_4)_3OH(s)$) crystallization is defined by Equation A1, as follows [6]:

$$\Delta\mu = KTln\,(1+\sigma) = KTln\frac{[a(Ca^{2+})]^5[a(PO_4^{3-})]^3[a(OH^-)]}{K_{so}(Hap)} \qquad (A1)$$

where K is the Boltzmann constant, T (K) is the absolute temperature, K_{so} is the solubility product, a is the activity of species i, and σ is the relative solution supersaturation index.

At a given $\Delta\mu$, natural nucleation is a kinetically controlled process in which the Hap nuclei overcome a homogeneous nucleation barrier ($\Delta G_{homo}{}^*$) [6] that could be estimated by Equation A2, as follows:

$$\Delta G_{homo}^* = \frac{16\pi\gamma_{cf}^3\Omega^2}{3[KT\ln(1+\sigma)]} \qquad (A2)$$

542   where γ_{cf} is the specific interfacial free energy between the crystals and the mother phase, and Ω

543   is the volume of the growth units.

544   The nucleation induction time (t_s) [7], [8] and [9] at different supersaturation levels could be used

545   to characterize the kinetics of nucleation and could be calculated by Equation A3, as follows:

546    $$ln\,t_s = \frac{k_n f(m)}{[\ln(1+\sigma)]^2} - ln\left(V R_s^2 N_0\, f^{"}(m)[f(m)]^{1/2} B\right) \qquad (A3)$$

547   where R_s is the crystal radius, N_0 is the mineral density, B is the kinetic constant, V is the solution

548   volume, and m is a factor that depends on the interaction and interfacial structural match between

549   the crystalline phase and substrate; it is expressed as a function of the interfacial free energy

550   difference among the different phases, as shown in Equation A4 as follows [10]:

551    $$m = \frac{\gamma_{sf} - \gamma_{sc}}{\gamma_{cf}} \quad (-1 < m < 1) \qquad (A4)$$

552   where γ_{sf}, γ_{sc}, and γ_{cf} correspond to the interfacial tension between substrate and fluid, crystal

553   and substrate, and crystal and fluid, respectively.

554   Furthermore, *f(m)* is the interfacial correlation factor describing the reduction of the nucleation

555   barrier ΔG^*_{homo} due to the occurrence of the substrate and is defined by Equation A5; *f"(m)* is the

556   pre-exponential term describing the ratio between the average effective collision in the presence

557   and absence of substrate and is defined by Equation A6. Finally, k_n is the nucleation constant,

558   which remains constant under a given condition m, and is defined by Equation A7.

559    $$f(m) = \frac{1}{4}(2 - 3m + m^3) \qquad (A5)$$

560    $$f''(m) = \frac{1}{2}(1 - m) \qquad (A6)$$

561    $$k_n = \frac{16\pi\gamma_{cf}^3 \Omega^2}{3(KT)^3} \qquad (A7)$$

562 For a crystalline phase m, f(m) takes only those values corresponding to some

563 crystallographically preferred orientations; then, it is possible according to Equation A3, to obtain

564 a set of intercepting straight lines by plotting ln t_s versus $1/[\ln (1+\sigma)]^2$. These lines with different

565 slopes k_nf(m) in the different regimes indicate that nucleation is governed by a sequence of

566 progressive heterogeneous processes, as described by Lamer and Dinegar (1950) [1].

Appendix references

567

568 [1]   LaMer.V. K. and Dinegar.R. H., Theory, ptoduction and mechanism of formation of
569   monodispersed Hydrosols, J. Am. Chem. Soc. 72 (1950) 4847–4854.

570 [2]   C. Destrée, F. Debuigne, L. Jeunieau, J.B. Nagy, Mechanism of formation of inorganic
571   and organic nanoparticles from microemulsions., Adv. Colloid Interface Sci. 123-126
572   (2006) 353–67.

573 [3]   R. Viswanatha, D.D. Sarma, Growth of Nanocrystals in Solution, 2007.

574 [4]   A.L. Sarode, P. Wang, S. Obara, D.R. Worthen, Supersaturation, nucleation, and crystal
575   growth during single- and biphasic dissolution of amorphous solid dispersions: polymer
576   effects and implications for oral bioavailability enhancement of poorly water soluble
577   drugs., Eur. J. Pharm. Biopharm. 86 (2014) 351–60.

578 [5]   Y. Sun, Controlled synthesis of colloidal silver nanoparticles in organic solutions: empirical
579   rules for nucleation engineering., Chem. Soc. Rev. 42 (2013) 2497–511.

580 [6]   A.C. Zettlemoyer, Nucleation, New York, NY: Dekker, 1969.

581 [7]   X.Y. Liu, Heterogeneous nucleation or homogeneous nucleation?, J. Chem. Phys. 112
582   (2000) 9949–9955.

583 [8]   Sato.K, Furukawa, Y. Nakajima, K, Advances in crystal growth research,: 2001, 42–61.

584 [9]   H. Jiang, X.-Y. Liu, G. Zhang, Y. Li, Kinetics and template nucleation of self-assembled
585   hydroxyapatite nanocrystallites by chondroitin sulfate., J. Biol. Chem. 280 (2005) 42061–
586   6.

587 [10]   H. Jiang, X.-Y. Liu, Principles of mimicking and engineering the self-organized structure of
588   hard tissues., J. Biol. Chem. 279 (2004) 41286–93.

589

Table

1   Table 1. Composition of industrial desalinated brines used in this study.

	Ca (g Ca(II)/L)	Na g Na(I)/L	Cl g Cl$^-$/L	SO$_4^{2-}$ g SO$_4^{2-}$/L	Mg^a g Mg(II)/L	pH$_{initial}$
Mg/Ca (2.2) brine	0.23	23.5	34.2	3.4	0.30	8.8
Mg/Ca (3.3) brine	0.41	18.9	16.4	20.1	0.85	8.9

2   a The Mg content is low because Mg(II) was recovered as Mg(OH)2

Figure

Figure captions:

2

3 Figure 1. Effect of pH on a) the P(V) concentration variation and b) the P(V) recovery by precipitation

4 using the Mg/Ca (2.2) brine, c) the P(V) concentration variation and d) the P(V) recovery by precipitation

5 using the Mg/Ca (3.3) brine (dotted line represents the expected P(V) concentration if any precipitation.

6

7 Figure 2. Variation concentration of major components (Mg(II), Ca(II), SO_4^{2-} and Cl^-) in experiments

8 under different pH conditions using the Mg/Ca (2.2) brine (solid lines are the total ion concentration

9 added throughout the precipitation experiment).

10

11 Figure 3. Saturation index (SI) for several minerals in the reactor for brine (Mg/Ca=2.2) at a) pH 11.5 for

12 Ca-phosphate minerals, b) pH 8 for Ca-phosphate minerals and c) pH 8 and 11.5 for Mg-phosphate

13 minerals.

14

15 Figure 4. XRD spectra of the particles obtained in the stirred batch reactor with Mg/Ca (2.2) brine a)

16 ACP at pH 9.5 and 11.5 and b) Crystal solid at different pH values after thermal treatment.

17

18 Figure 5. Variation of major components (Mg(II), Ca(II), SO_4^{2-} and Cl^-) in the batch experiments under

19 different pH conditions using the Mg/Ca (3.3) brine (solid lines are the total ion concentration added

20 along the precipitation experiment).

21

22 Figure 6. XRD spectra of the particles produced in the stirred batch reactor with Mg/Ca (3.3) brine at a)

23 pH 11.5 and 9.5 and b) pH 9.5 amorphous solid and c) pH 9.5 after thermal treatment of amorphous
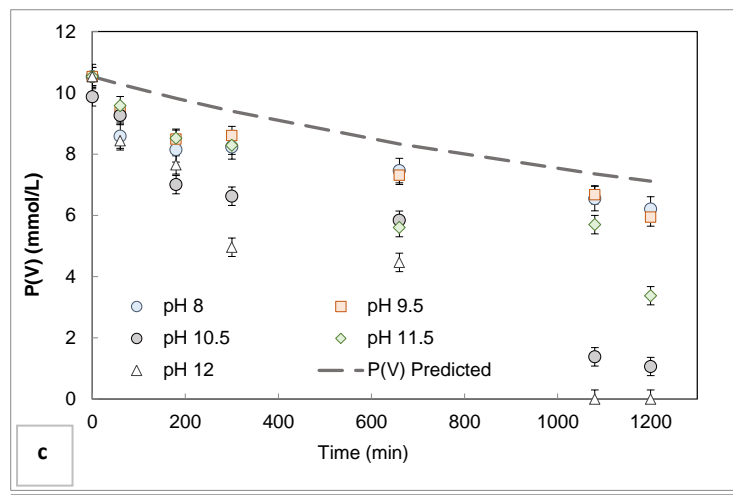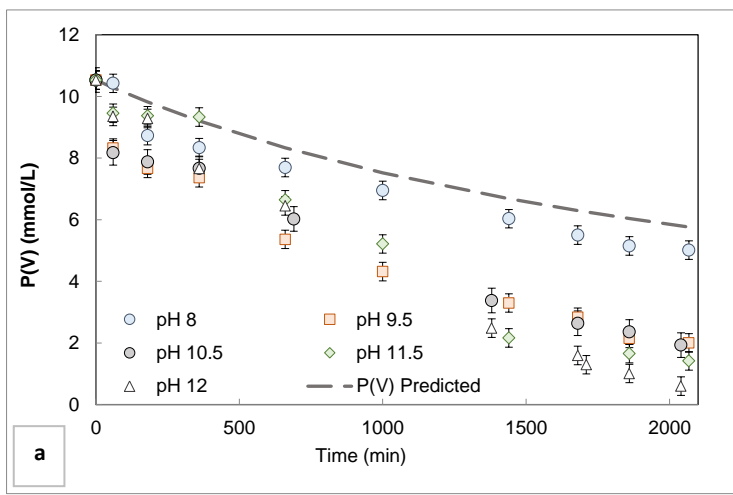
24 precipitates.

25

26 Figure 7. Supersaturation index (SI) for Ca/Mg (2.2) brine with respect to Hap at different pH values (8,

27 9.5 and 11.5) as a function of precipitation time in the batch reactor.
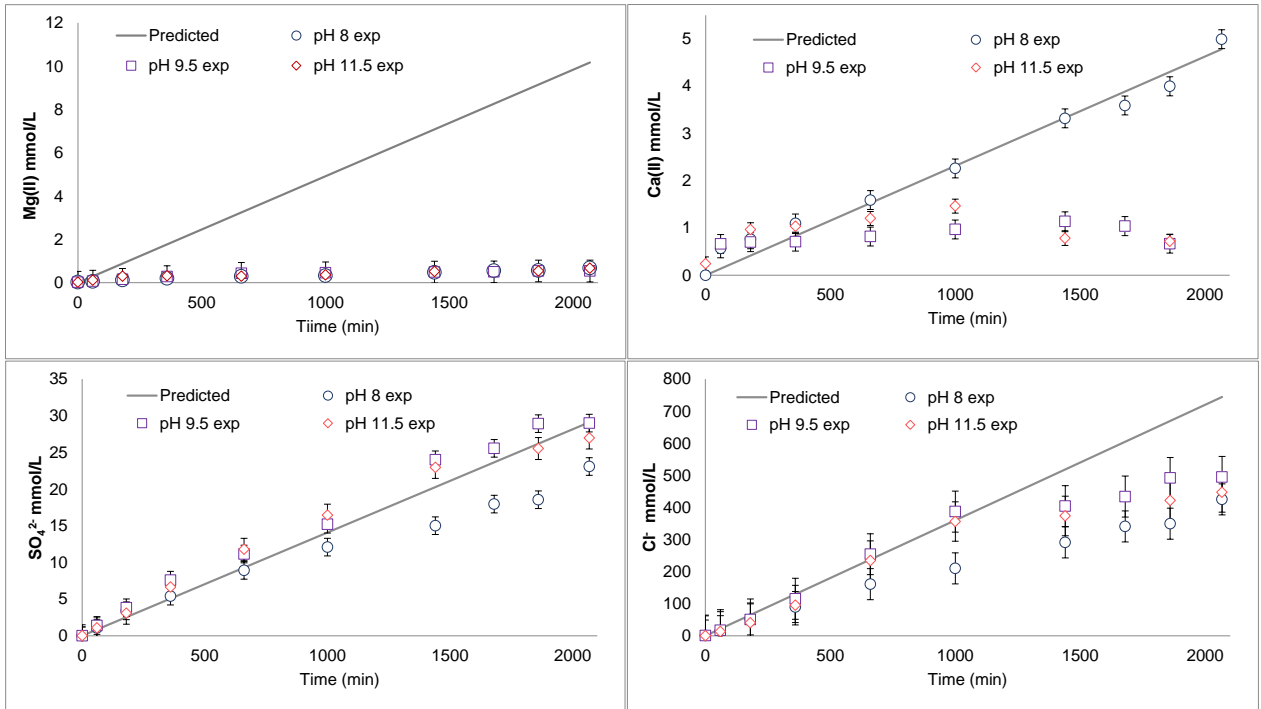
28

29 Figure 8. Evaluation of the nucleation kinetics using the dependence of $\ln(t_s)$ versus $1/[\ln(1+\sigma)]^2$ [47] for

30 Hap nucleation with Mg/Ca (2.2) brine at different pH values (8 and 9.5).

1
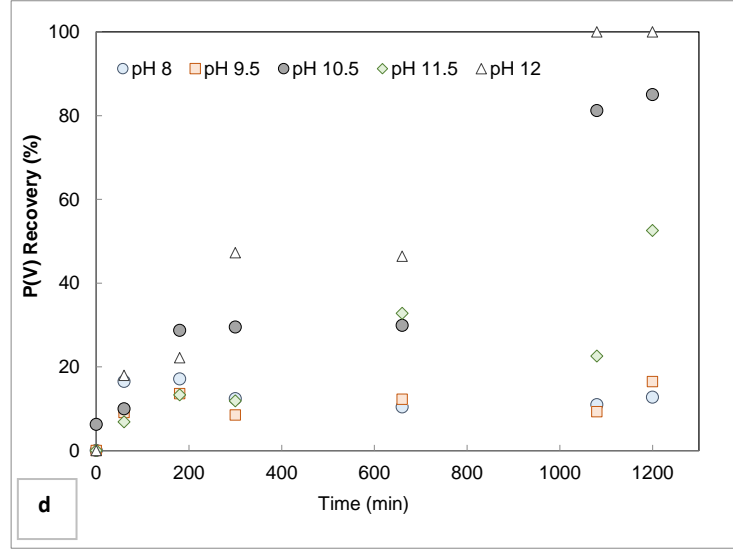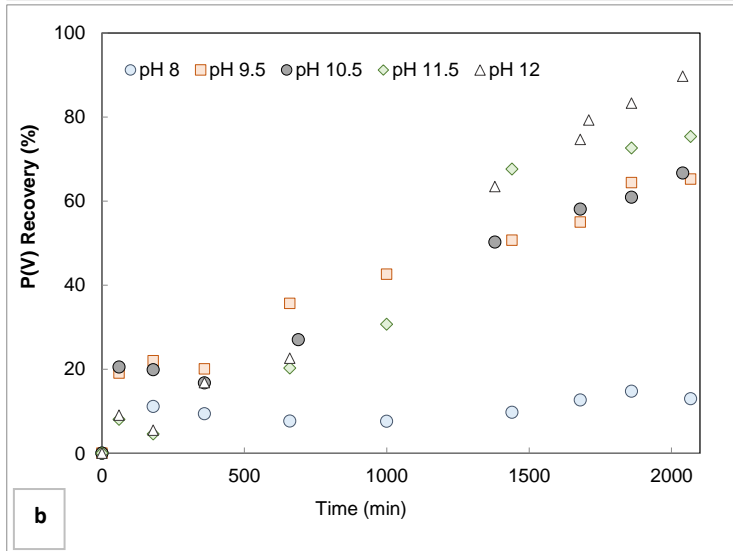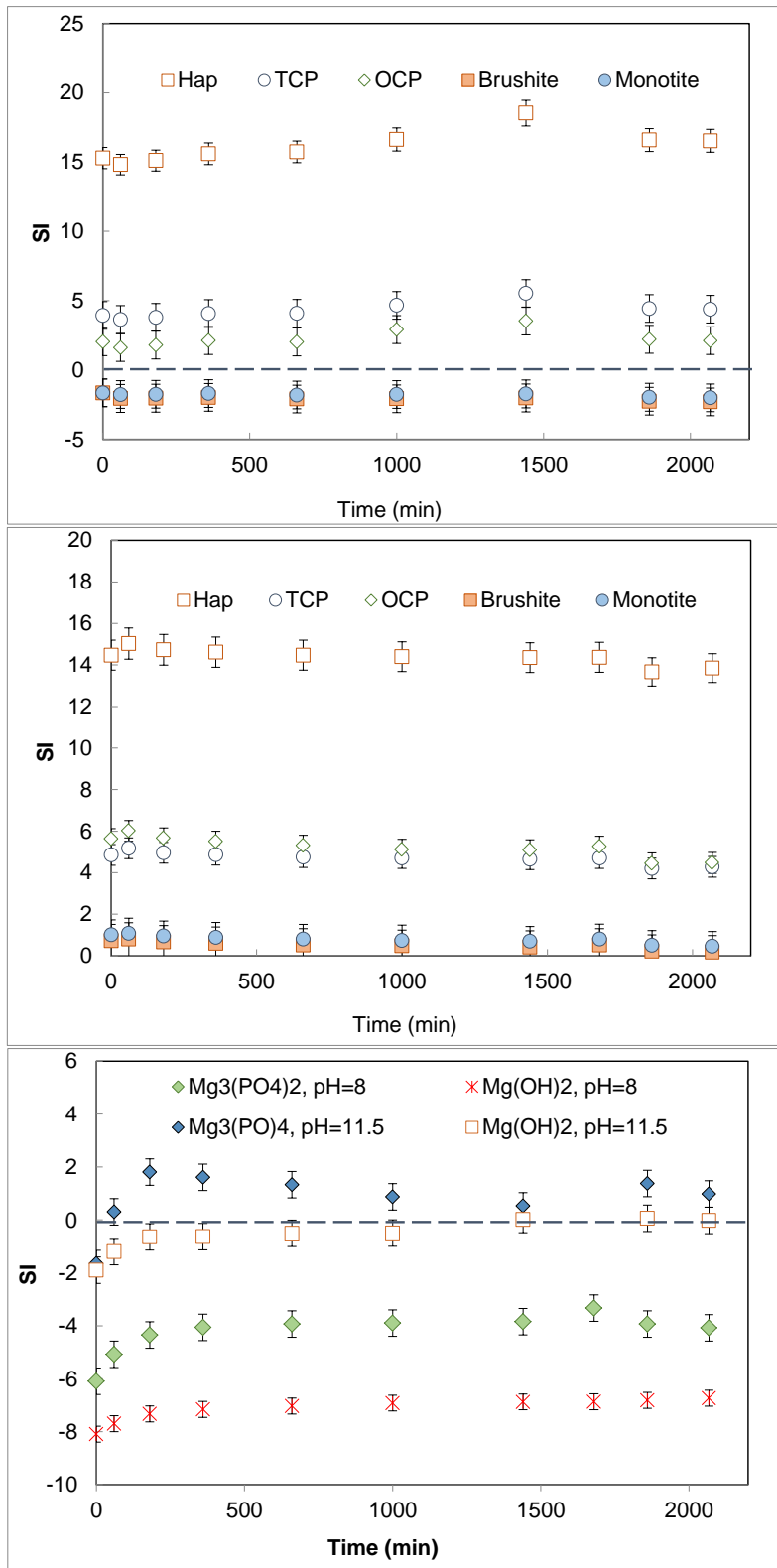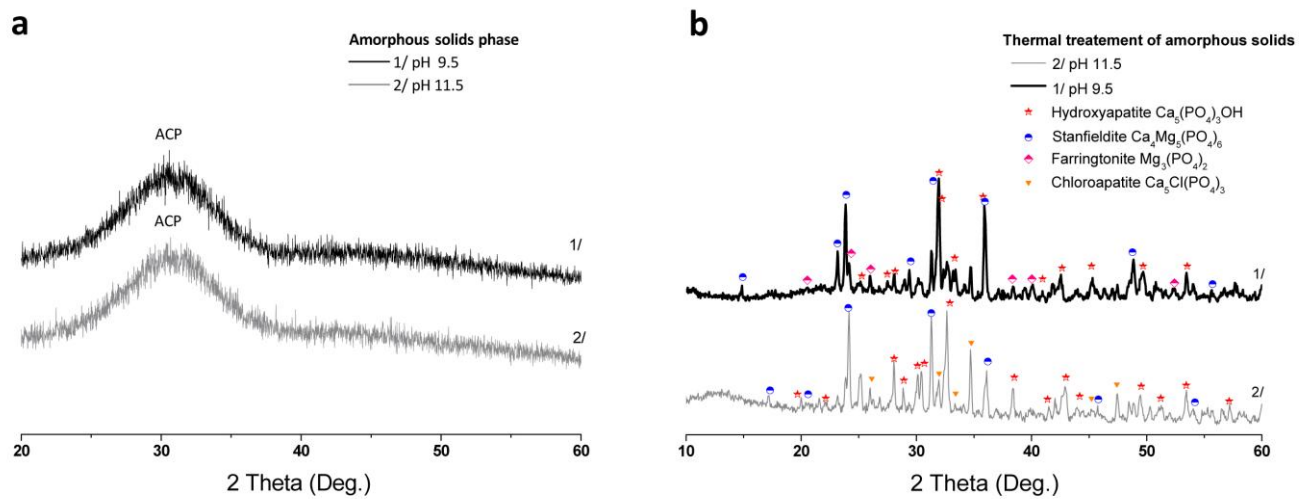

2   Figure 1.

3

4   Figure 2.

5

6

7   Figure 3.
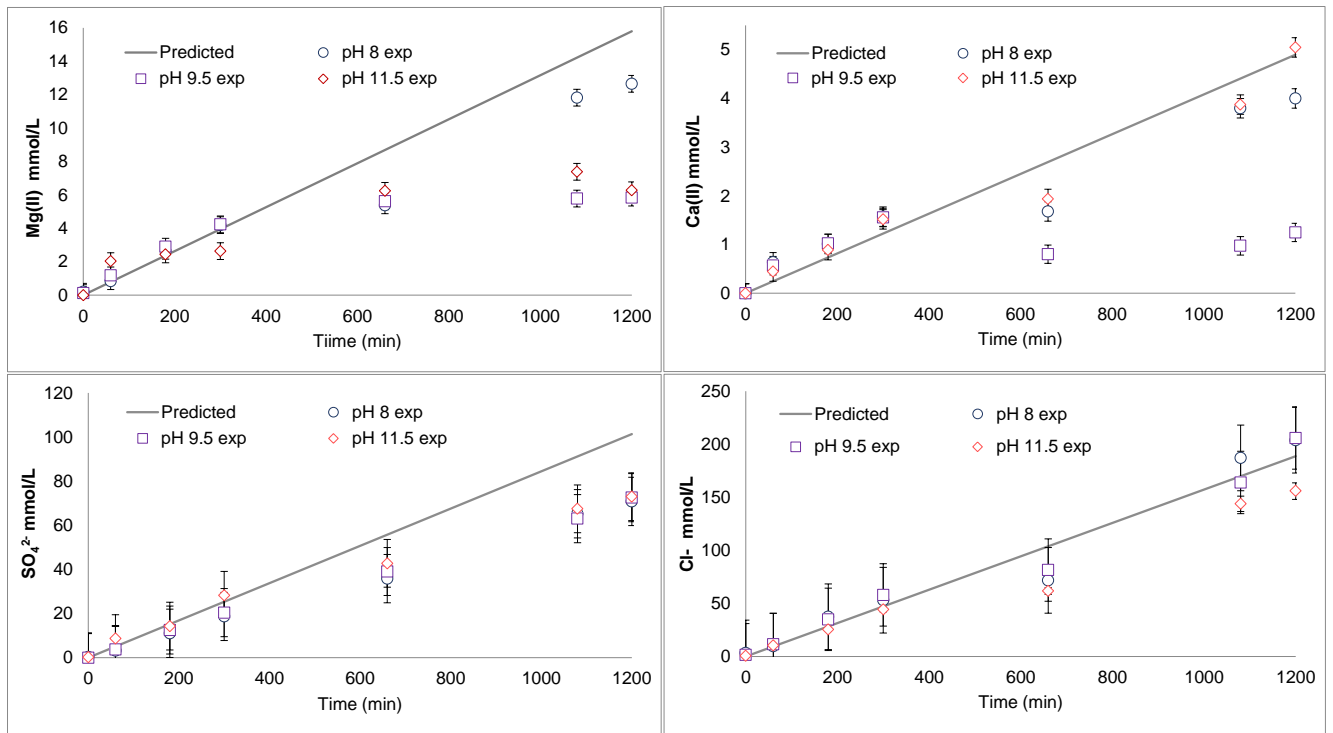
8

9

10   Figure 4.

11

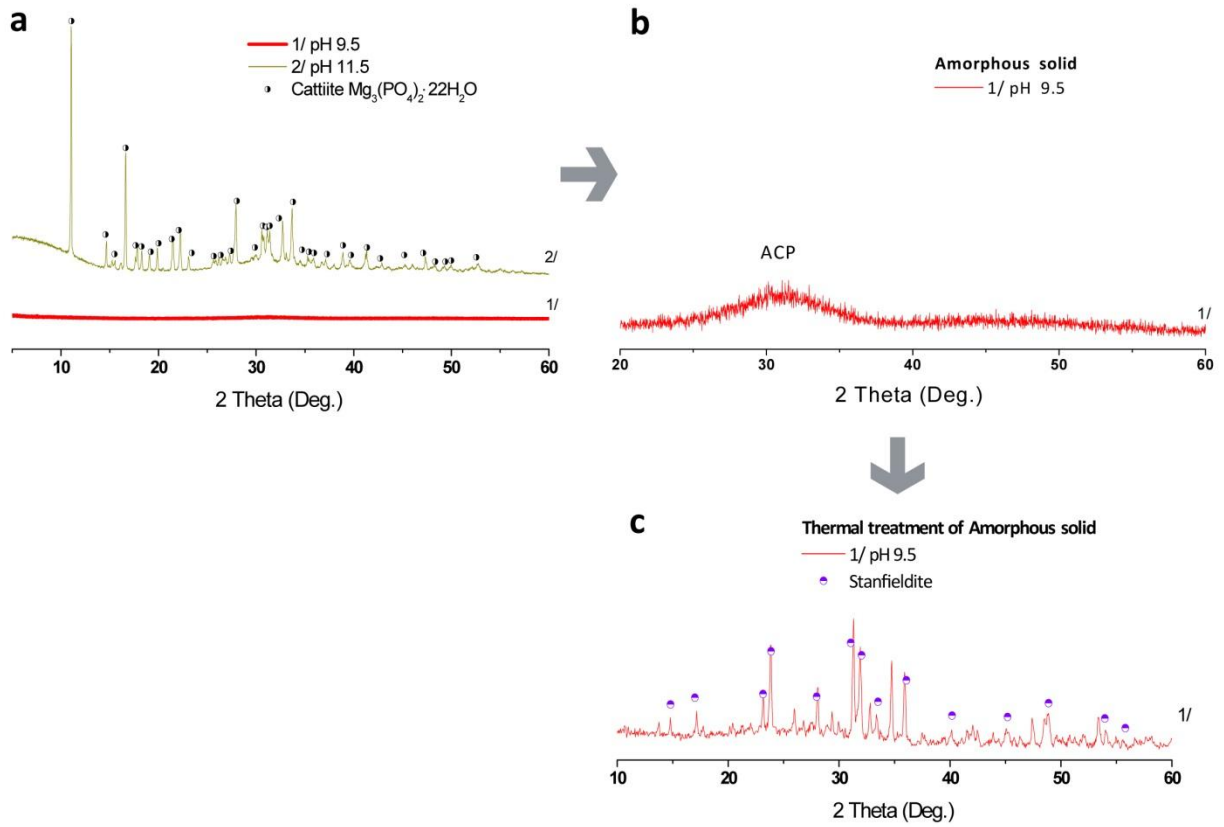12

13

14

15

16

17

18

19

20   Figure 5.

21

22

23
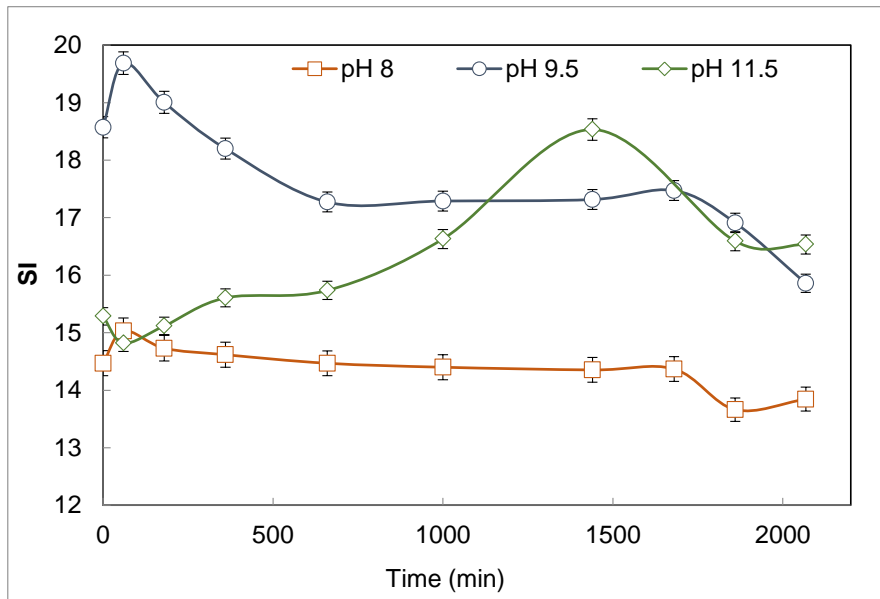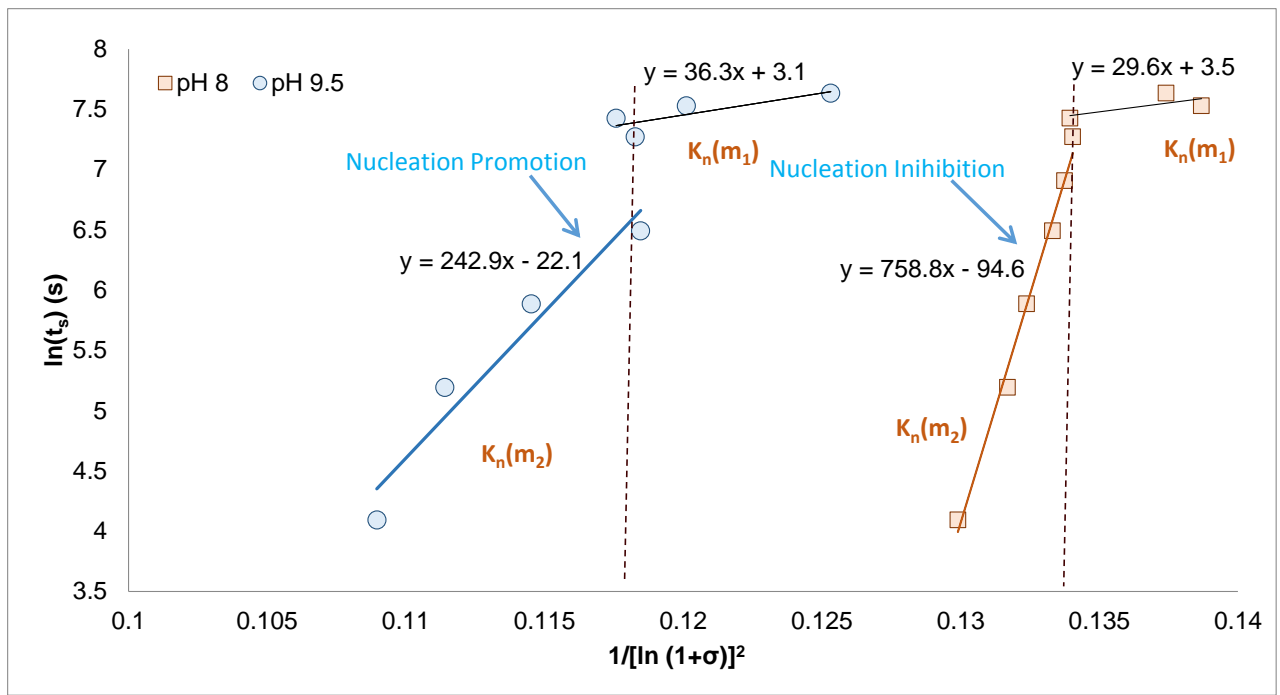
Figure 6.

24

25

26

27

28

29

30

31

32

33

Figure 7.

34

35

36

37

38

39

40

41

42

43

Figure 8.